Modeling of Magnetizing Inductance and Leakage Inductance in a Matrix Transformer

Khai D. T. Ngo, *Member, IEEE,* E. Alpizar, and J. Kenneth Watson, *Senior Member, IEEE*

***Abstract*—Winding and core geometries are described for a matrix transformer constructed from integrated core and z-folded flex circuits. The magnetizing inductance is derived using reluctance method and exploiting structural periodicity and symmetry. The internal leakage inductance is computed from magnetic field distribution and the interconnect leakage inductance from inductance formulas and current distribution. The results show that the interconnects are responsible for most of the leakage inductance. The modeling approaches predict inductance values that agree well with experimental measurements.**

I. Introduction

THE "matrix transformer" was introduced in [1], [2] as a viable approach to realize low-profile, high-density, distributed magnetic components. In its simple form, a matrix transformer can be constructed from discrete cores and magnet wire (which may be round or square, and solid or Litz). It can also be constructed from an integrated core and flexible circuits for further reduction in volume and height [3].

Several practical issues associated with the integrated-core/flex-circuit construction were addressed in [3], including core geometry, winding geometry, design procedure, and fabrication processes. The design procedure was based primarily on winding loss and core loss optimization. Preliminary experimental results were also reported. Inductance calculations, however, were not covered.

This paper reports the results of magnetizing and leakage inductance modeling for the integrated-core/flex-circuit matrix transformer. This modeling was motivated by several factors. First, equations relating inductances to transformer geometry and material characteristics need to be developed so that the matrix transformer could be designed for a given magnetizing inductance and leakage inductance, which are an integral part of the operation of several resonant-type converters [4]. Second, a methodology to compute inductances that is applicable to the matrix transformer needs to be formulated since the geometry of the matrix transformer is quite unique. Third, an inductance model needs to be developed to substantiate the expectation that a matrix transformer may offer high magnetizing inductance and low leakage inductance.

Manuscript received June 14, 1991; revised September 18, 1992. This research was supported in part by IBM Corp., Federal Sector Division, Owego, NY 13827-1228 under contract 425310, and by the National Science Foundation under grant ECS-8957926.

K. D. T. Ngo and J. K. Watson are with the Department of Electrical Engineering, University of Florida, Gainesville, FL 32611.

E. Alpizar are with the Instituto Tecnologico de Costa Rica. He is now with the Escuela de Ingeniería Electrica de Universidad de Costa Rica.

IEEE Log Number 9206664.

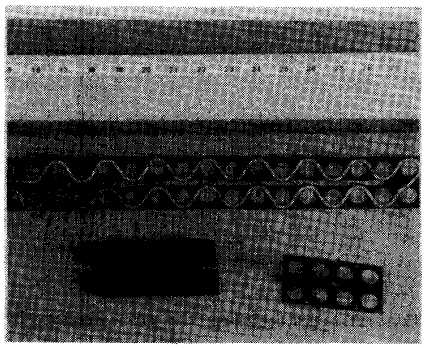

Fig. 1. Clockwise: core pieces, primary winding, and secondary winding of a 4 × 2 matrix transformer.

To facilitate the explanation, the modeling techniques are demonstrated for the 4 × 2 matrix transformer presented in [3]. The *core geometry* and *winding geometry* of this 4 × 2 matrix transformer are reviewed in Section II. Geometric information and material properties are then used to derive the equation describing the *magnetizing inductance* in Section III. The equations modeling the *leakage inductance,* which consists of an "internal" component and an "interconnect" component, are derived in Section IV. The analytical results are verified experimentally in Section V. Essential results are summarized in the concluding section.

II. Description of Matrix Transformer Geometry

As its name implies, the 4 × 2 matrix transformer [3] is the integration at both the core and winding levels of eight elemental transformers into two rows, each row having four elemental transformers. The components of the transformer before assembly are shown in Fig. 1, which shows two ferrite core pieces in the right upper half of Fig. 1, as well as two flex circuits: a long one in the lower half of Fig. 1 for the primary winding and a short one in the left upper half of Fig. 1 for the secondary winding.

A. Transformer Core

The complete core consists of a *top plate* and a *bottom plate,* which are bridged by two rows of ferrite *posts,* each row containing four cylindrical posts and two semicylindrical posts. To reduce fabrication cost and to facilitate testing, however, the core is constructed from four identical *core pieces* like the ones shown in Fig. 1.

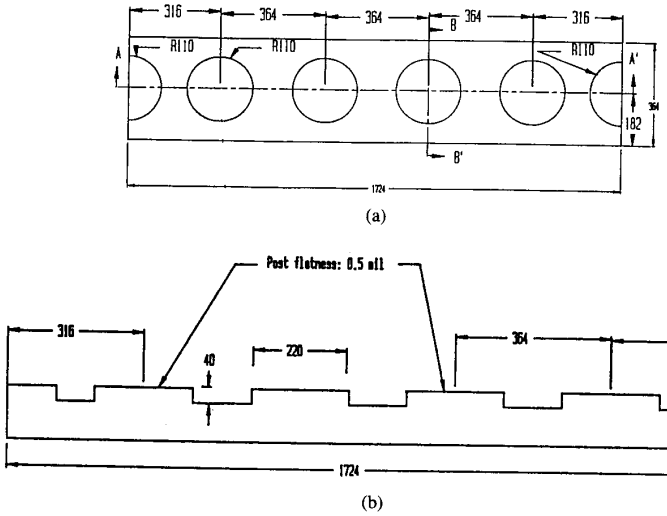

Fig. 2. Mechanical drawings for each core piece (dimensions in mils). (a) Top view. (b) Section A-A′.

It can be seen that each core piece contains a plate, four cylindrical posts, and two semicylindrical posts (at the two ends). Each semicylindrical post completes the path for half of the flux in the adjacent cylindrical post. The semicylindrical posts help preserving "magnetic periodicity," which means that the matrix transformer may be decomposed into identical (or almost-identical) magnetic elements. As is evident shortly, this magnetic periodicity simplifies the modeling of magnetizing inductance.

The top or bottom plate is constructed by placing two core pieces side by side as shown in Fig. 1. The complete core is realized when the top and bottom plates are assembled such that the surfaces of the respective (semi-) cylindrical posts contact. The dimensions in mils (one-thousandth of an inch) in each core piece are shown in Fig. 2.

B. Primary Winding

Since the operating frequency of the transformer is 1 MHz, it is not advantageous for the primary and secondary windings to be significantly thicker than twice the skin depth of copper at 1 MHz. Thus, the winding thicknesses are generally less than 5 mil. Therefore, the windings were fabricated from *flex circuits* explained as follows.

Fig. 1 shows the flex circuit for the primary winding, which is a *serpentine pattern of copper* etched on an *insulating laminate*. The serpentine pattern consists of 32 half-turns, which are equivalent to 16 full turns, automatically connected in series. It curves around *large apertures* etched out of the insulating laminate. These large apertures provide the passages for the ferrite posts. The *small apertures* located along the top and bottom edges of the flex circuit are *alignment markers*.

Ignoring the secondary winding for now, the primary winding is realized by "z-folding" the flex circuit at the first folding line, which is located between the second (counted from the left edge of the flex circuit) and third alignment markers (small apertures); then at the second folding line, which is located between the fourth and fifth alignment marker; and finally at the third folding line, which is located between the sixth and seventh alignment markers. Thus, the primary winding consists of four copper/insulator layers. When the primary winding assembly is dropped onto the bottom plate and covered by the top plate, each cylindrical post is encircled by two complete turns which are composed of four half-turns, each half-turn contributed by one layer. The typical dimensions for the primary flex circuit are shown in Fig. 3. The copper thickness is 2.8 mil and the insulation thickness is 2 mil.

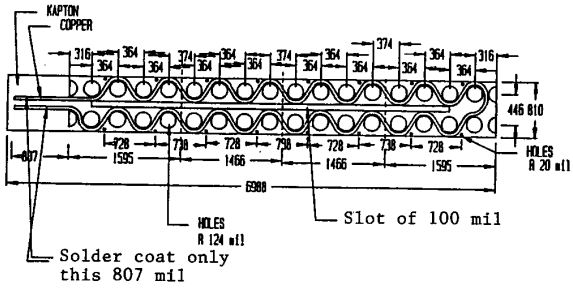

Fig. 3. Mechanical drawings for the unfolded primary flex circuit (dimensions in mils). Outer coil radius: 182 mil; inner coil radius: 132 mil; copper thickness: 2.8 mil; insulation thickness: 2 mil.

C. Secondary Winding

The secondary winding has *one* turn, which is actually the *parallel combination* of eight turns from eight elemental transformers. The eight turns are etched on the secondary flex circuit as shown in Fig. 4. It can be seen that most of the paralleling connections are already in place. Some external connections, however, are required to complete the paralleling and to add the terminations. Short copper stubs (labeled "SC" in Fig. 4) are thus added to the flex circuit to facilitate the soldering of these external connections. The left, center, and right stubs are paralleled by one copper strip, and

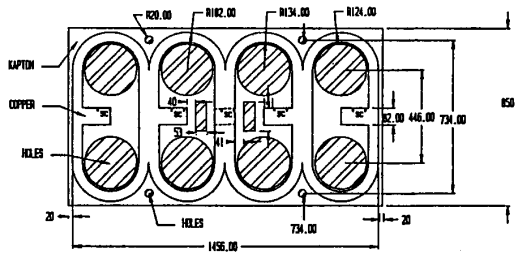

Fig. 4. Mechanical drawings for the secondary flex circuit. Solder coat is on terminals marked "sc." Copper thickness: 4.2 mil; insulation thickness: 2 mil. All dimensions are in mils.

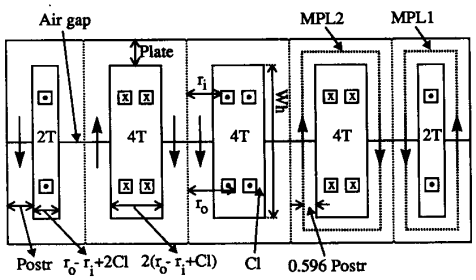

Fig. 5. Cross-section of one row of transformers for computing the magnetizing inductance.

the remaining stubs by another copper strip. Terminations are added to the center of these paralleling strips.

To reduce eddy-current losses, the secondary flex circuit is *interleaved* between the second and third layers of the primary flex circuit. The typical dimensions for the secondary flex circuit are shown in Fig. 4. The copper thickness is 4.2 mil and the insulation thickness is 2 mil.

III. Modeling of the Magnetizing Inductance

The magnetizing inductance is measured across the primary winding while the secondary winding is open circuited. The modeling of the magnetizing inductance of a matrix transformer could be complex because there are several flux paths that appear to be coupled magnetically. Fortunately, thanks to the *magnetic periodicity* introduced into the structure during fabrication, the matrix transformer may be decomposed into several identical (or almost-identical) magnetic elements which may be treated as *uncoupled* magnetically. The magnetizing inductance for each element may then be computed and summed to calculate the overall magnetizing inductance.

To understand how the matrix transformer can be decomposed into uncoupled magnetic elements, consider the cross-sectional view of one row of posts and primary turns shown in Fig. 5. It can be seen that there are four posts, which have the same width (or cross-sectional area), and two semiposts, which have half the width of the other posts. There are also five winding windows. Three of these windows have the same width while the other two have half the width of the first three. Each larger winding window has four primary turns (since there are two primary turns for each post), whereas each smaller window has only two primary turns. The currents in adjacent windows flow in opposite directions. Consequently, the fluxes in adjacent posts flow in opposite directions.

If all the winding windows had the same width and the same number of turns, the magnetic structure may be decomposed into five *identical* magnetic elements by the four dashed lines coincident with the axes of symmetry of the posts, as shown in Fig. 5. Since the right and left elements have half the number of turns and approximately half the width of the other elements, slight asymmetry is introduced. This asymmetry, fortunately, is accounted for by the modeling approach described shortly.

Assuming that the flux in each magnetic element is uniform, the inductance $L_{m1(2)}$ of the element with mean path length MPL1(2) (see Fig. 5) may be computed by [7]:

$$L_{m1} = \frac{N_1^2}{R_{m1} + R_g} \quad \text{or} \quad L_{m2} = \frac{N_2^2}{R_{m2} + R_g} \tag{1}$$

where

$$R_g \approx \frac{1}{\mu_o}\frac{2g}{S_{\text{path}}} \quad \text{and} \quad R_{m1} \approx \frac{1}{\mu}\frac{\text{MPL1}}{S_{\text{path}}} \quad \text{or} \quad R_{m2} \approx \frac{1}{\mu}\frac{\text{MPL2}}{S_{\text{path}}} \tag{2}$$

where

$$S_{\text{path}} = (2\text{Postr})(\text{Plate}) = \tfrac{1}{2}\pi(\text{Postr})^2 \tag{3}$$

$$\text{MPL1} = 2(1.192\,\text{Postr} + r_o - r_i + 2\text{Cl} + \text{WH} + \text{Plate}) \tag{4}$$

$$\text{MPL2} = 2(1.192\,\text{Postr} + 2(r_o - r_i + \text{Cl}) + \text{WH} + \text{Plate}). \tag{5}$$

(Unless otherwise specified, MKS (meter-kilogram-second) units are used in all equations.) In (1), $N_{1(2)}$ is the number of turns ($N_1 = 2$ and $N_2 = 4$ in Fig. 5); $R_{m1(2)}$ is the reluctance of the ferrite path; and R_g is the reluctance of the air gaps in series with the ferrite path. (The air gaps are usually present at the mating surfaces of the upper and lower halves of the cores.) In (2), μ_o is the permeability of air; μ is the permeability of ferrite; g is the length of the air gap in each post; and S_{path} is the cross-sectional area of the magnetic path. The variables in (3)–(5) are defined in Fig. 5: Postr is the post radius; Plate is the thickness of the top or bottom plate; r_o and r_i are the outer and inner radii of each turn, respectively; C1 is the clearance between the winding and the core; and WH is the height of the winding window. The origins of (3)–(5) are explained below.

The first equality in (3) expresses S_{path} as the area of the *rectangular* cross-sections of the magnetic paths along the top and bottom plates. The dimensions of these cross-sections are 2*Postr, the diameter of the posts, and Plate, the thickness of the plates. The second equality in (3) expresses S_{path} as half of the cross-sectional area of the cylindrical posts. The two equalities in (3) are enforced during design and fabrication.

MPL1(2) is the perimeter of the dashed rectangle which represents the mean path length. The horizontal sides of the MPL1(2) rectangle are at a distance Plate/2 away from the corresponding horizontal sides of the winding window.

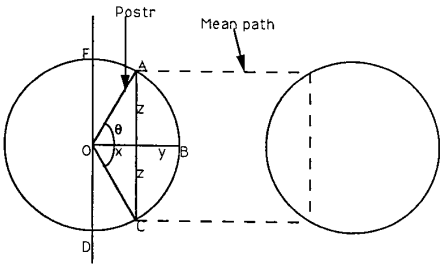

Fig. 6. Top view of two adjacent cylindrical posts and the mean flux path.

The vertical sides of the MPL1(2) rectangle are located at a distance $y = 0.596$*Postr away form the corresponding vertical sides of the winding window. It can be proved from Fig. 6, which shows the top view of two adjacent posts and the associated mean flux path, that this distance will make the area ABC to be half of the post area $ABCDOF$. The constant 1.192 in (4) is 2*.0596.

If there are n_1 magnetic elements of magnetizing inductance L_{m1} and n_2 elements of magnetizing inductance L_{m2}, the total magnetizing inductance is

$$L_{mt} = n_1 L_{m1} + n_2 L_{m2} \tag{6}$$

For the 4 × 2 matrix transformer with $n_1 = 4, n_2 = 6$, $N_1 = 2$, and $N_2 = 4$:

$$L_{mt} = \mu * \text{Postr} * \text{Plate} * \left(\frac{32}{\text{MPL1} + 2\mu_r g} + \frac{192}{\text{MPL2} + 2\mu_r g} \right) \tag{7}$$

where $\mu_r = \mu/\mu_o$ is the relative permeability of ferrite. The above equation will be verified experimentally later.

IV. Modeling of the Leakage Inductance

The leakage inductance is measured across the primary winding while the secondary winding is short circuited. It is postulated that this inductance consists of an "internal" component and an "interconnect" component. The internal leakage inductance is computed from the energy [5] stored in the "internal" volume that contains *both* the primary and secondary turns, but excludes the two strips that parallel the secondary turns. The interconnect leakage inductance is computed from the energy stored in the "interconnect" volume, which consists primarily of the paralleling strips. (By overlaying Figs. 3 and 4, it can be seen that there are secondary winding segments that are outside the "internal" volume defined by Fig. 5 and thus belong to the "interconnect" volume. The inductances contributed by these winding segments, however, are neglected in the following analysis although they can be computed by the appropriate equations described below.)

A. Internal Leakage Inductance

In general, the magnetic energy E associated with a media can be computed by

$$E = \frac{1}{2} \int_{\text{volume}} \boldsymbol{B} \cdot \boldsymbol{H}\, dv = \frac{\mu}{2} \int_{\text{volume}} H^2 dv \tag{8}$$

where $\boldsymbol{B}$ and $\boldsymbol{H}$ are the magnetic flux density and magnetic field intensity, respectively; μ is the permeability of the media; and dv is the differential volume. The above integration is negligible in the core volume because the short-circuited secondary winding renders the fields inside the core negligible. Thus, it is only necessary to find E or $\boldsymbol{H}$ in the *winding windows* in Fig. 5.

The procedure to calculate $\boldsymbol{H}$ is now demonstrated for the simplified winding window shown in Fig. 7. Assuming that the winding windows possess 2D (two-dimensional) axisymmetry and neglecting fringing at the window boundaries, $\boldsymbol{H}$ may be approximated by

$$\boldsymbol{H} = H_r(r, z)\hat{\boldsymbol{r}} \tag{9}$$

where $\hat{\boldsymbol{r}}$ is the unit radial vector. To satisfy Gauss' law [8], H_r should vary inversely with r at a given z:

$$H_r(r, z) = \frac{f(z)}{r}. \tag{10}$$

To determine $f(z)$ *within a conductor*, Ampere's law [8] may be applied along Ampere's contour shown in Fig. 7:

$$\oint \boldsymbol{H} \cdot d\boldsymbol{l} = \int_{\text{surface}} \boldsymbol{J} \cdot ds \tag{11}$$

where $\boldsymbol{J}$ is the surface current density; $d\boldsymbol{l}$ is the differential length along the contour; and ds is the differential surface area. Neglecting the clearance between the conductor and the core, the integral on the left side of the preceding equation is reduced to the integration of H_r along the segment at z and between r_i and r_o shown in Fig. 7, for H_r is negligible outside this segment. If the conductor is sufficiently thin so that the current in the conductor is approximately uniform in the z direction, the integral on the right side is Iz/t, where I is the total current in the conductor and t the conductor thickness. The preceding equation then yields

$$\int_{r_i}^{r_o} \frac{f(z)}{r} dr = \frac{Iz}{t} \Rightarrow f(z) = \frac{Iz}{t \ln(r_o/r_i)}. \tag{12}$$

Equation (10) then becomes

$$H_r(r, z) = \frac{I}{t \ln(r_o/r_i)} \frac{z}{r} \quad \text{for} \quad 0 \le z \le t, r_i \le r \le r_o. \tag{13}$$

In the *separation region* between two adjacent conductors where $t \le z \le t'$ (see Fig. 7), H_r is constant with respect to z since Ampere's contour drawn for this region always encloses a constant current I. Since H_r is continuous across the conductor surface at $z = t$, the preceding equation may be evaluated at $z = t$ to give

$$H_r(r, z) = \frac{I}{\ln(r_o/r_i)} \frac{1}{r} \quad \text{for} \quad t \le z \le t', r_i \le r \le r_o. \tag{14}$$

The foregoing procedure can be extended to find $\boldsymbol{H}$ in the winding windows shown in Fig. 5. Note, however, that although the definitions of "winding windows" and "identical magnetic elements" used in Section III facilitate the modeling of magnetizing inductance, they do not possess

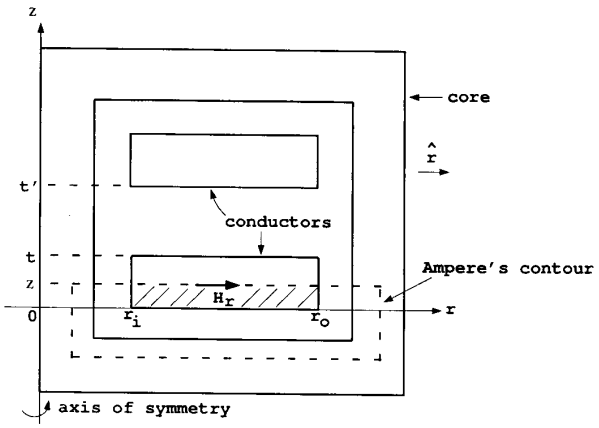

Fig. 7. Ampere's contour to determine the dependence of $H_r(r, z)$ on z.

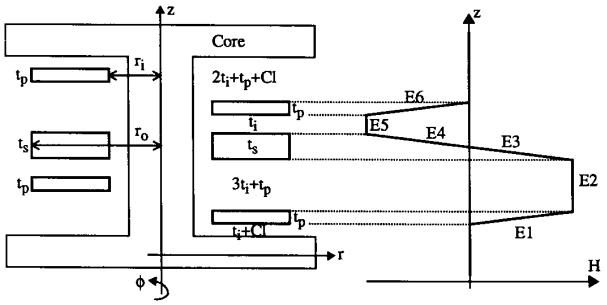

Fig. 8. (a) Windings and their locations within a winding window. (b) Variation of H_r with z.

the 2D axisymmetry exemplified in Fig. 7, which is more convenient in the modeling of leakage inductance. Therefore, the "identical magnetic element" is redefined in Fig. 8(a) along with its center post and "winding window." Each window then contains two primary turns with thickness t_p and one secondary turn with thickness t_s. The separations among the turns are delineated in terms of t_p and t_s, as well as the insulating thickness t_i. (The clearance C1 between the core and the winding assembly does not enter the calculation.)

Since the secondary winding is short circuited, $-2I$ flows in the secondary turn if I flows in each primary turn. The variation of H_r with respect to z is then as shown in Fig. 8(b). The linear variations in the regions occupied by the conductors are governed by (13), the signs of the slopes dictated by the signs of the currents. The constant values of H_r in the separation regions are governed by (14).

Substituting equations like (13) and (14) into (8) and performing the integration yield the following equations for energy for all the regions:

$$E_1 = E_6 = \frac{I^2\pi\mu_o t_p}{3\ln(r_o/r_i)} \qquad E_2 = \frac{I^2\pi\mu_o(3t_i+t_p)}{\ln(r_o/r_i)} \tag{15}$$

$$E_3 = E_4 = \frac{I^2\pi\mu_o t_s}{6\ln(r_o/r_i)} \qquad E_5 = \frac{I^2\pi\mu_o t_i}{\ln(r_o/r_i)} \tag{16}$$

where μ_o is the permeability of the winding window. Since the internal magnetic energy E_{int} and the internal leakage inductance $L_{1,\text{int}}$ are related by

$$E_{\text{int}} = N_l(2E_1 + E_2 + 2E_3 + E_5) = \tfrac{1}{2}L_{l,\text{int}}I^2 \tag{17}$$

where N_l is the number of magnetic elements, which is eight for the 4 × 2 matrix transformer. The internal leakage inductance, measured across the primary winding with the secondary winding short-circuited, is then

$$L_{l,\text{int}} = \frac{16\pi\mu_o}{\ln(r_o/r_i)}\left(\frac{5}{3}t_p + \frac{1}{3}t_s + 4t_i\right). \tag{18}$$

B. Interconnect Leakage Inductance

The interconnect leakage inductance is associated with the strips which parallel the secondary turns. Fig. 9 shows the secondary turns, the paralleling strips, and the corresponding current distributions. It can be seen that there is a long strip that parallels terminations a, a', and $a''$and a short strip that parallels terminations b' and b''. Points a and b are where the two strips are shorted together for short-circuit tests. Although the strips are shown side-by-side for clarity, the long strip is actually placed directly on top of the short one such that their cross-sections are as arranged in Fig. 10. With I flowing in the primary turns and $2I$ in each secondary turn, $4I$ flows in the long strip and $8I$ in the short strip as shown in Fig. 9.

The interconnect leakage inductance $L_{l,\text{inc}}$ due to the paralleling strips can be computed from the magnetic energy and inductance formulas given in [6]. Let L_1 be the self-inductance of $a'a$ or aa'', L_2 be the self-inductance of $b'b$ or bb'', M_{12} be the mutual inductance between $a'a$ and $b'b$, M_{13} be the mutual inductance between $a'a$ and aa'', M_{14} be the mutual inductance between $a'a$ and bb'', and M_{24} be the mutual inductance between $b'b$ and bb''. These *interconnect inductances* are related to $L_{l,\text{inc}}$ via the magnetic energy formulas:

$$E_{\text{inc}} = \frac{L_{l,\text{inc}}I^2}{2} = L_1I_1^2 + L_2I_2^2 + 2M_{14}I_1I_4 - 2M_{12}I_1I_2 - M_{24}I_2I_4 - M_{13}I_1I_3 \tag{19}$$

With $I_1 = I_3 = 4I$ and $I_2 = I_4 = 8I$ as shown in Fig. 9:

$$L_{l,\text{inc}} = 32(L_1 + 4L_2 + 4M_{14} - 4M_{12} - 4M_{24} - M_{13}). \tag{20}$$

The interconnect inductances can generally be computed from (1) of [6] for the mutual inductance $M(l_t, G)$ of two parallel filaments of length l_t and at a distance G apart:

$$M(l_t, G) = 2\left[l_t \ln\left(\frac{l_t + \sqrt{l_t^2+G^2}}{G}\right) - \sqrt{l_t^2+G^2} + G\right]\text{nH} \tag{21}$$

where l_t and G are in centimeters (cm) and M is in nanohenrys (nH). The self-inductance $L_1\,(L_2)$ of the strip of length $a'a\,(b'b)$, width B, and thickness C is equal to the mutual inductance of two parallel filaments of length $a'a\,(b'b)$, which are separated by the "geometric mean radius" GMR of the rectangular cross-section of the strip:

$$L_1 = M(a'a = 4r_o, \text{GMR}) \qquad L_2 = M(b'b = 2r_o, \text{GMR}) \tag{22}$$

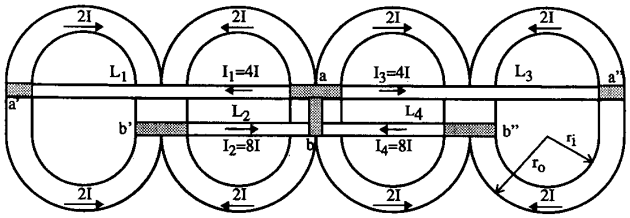

Fig. 9. Strips that parallel the secondary terminations and their current distributions.

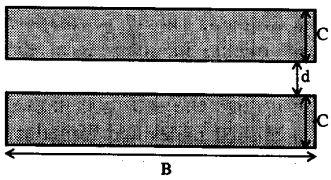

Fig. 10. Cross-sections of the paralleling strips.

where

$$\text{GMR} = 0.2235(B + C). \tag{23}$$

The mutual inductance M_{12} of the strips of length $a'a$ and $b'b$, width B, and thickness C is given by (33) of [6]:

$$2M_{12} = M(a'a, \text{GMD}) + M(b'b, \text{GMD}) - M(a'a - b'b, \text{GMD}) \tag{24}$$

$$M_{12} = .5M(a'a = 4r_o, \text{GMD}) \tag{25}$$

where the "geometric mean distance" GMD of the cross-sections defined in Fig. 10 is given by the following equation, derived from Table 2 of [6] by curve fitting, for planar conductors with $C/B < 0.1$:

$$\text{GMD} = B\exp\left[-1.50 + 3.06\left(\frac{C+d}{B}\right) - 3.37\left(\frac{C+d}{B}\right)^2 + 3.73\left(\frac{C+d}{B}\right)^3 - 2.20\left(\frac{C+d}{B}\right)^4\right] \tag{26}$$

where all dimensions are in centimeters. Mutual inductance M_{14} is given by (34) of [6]:

$$2M_{14} = M(a'a + bb'', \text{GMD}) - M(a'a, \text{GMD}) - M(bb'', \text{GMD}) \tag{27}$$

$$M_{14} = 0.5[M(6r_o, \text{GMD}) - M(4r_o, \text{GMD}) - M(2r_o, \text{GMD})]. \tag{28}$$

Mutual inductances M_{13} and M_{24} are calculated from (36) of [6]:

$$M_{13} = 8r_o \ln 2\,[\text{nH}] \qquad M_{24} = 4r_o \ln 2\,[\text{nH}] \tag{29}$$

where r_o is in centimeters (cm). The *total leakage inductance* is the sum of $L_{l,\text{int}}$ described by (18) and $L_{l,\text{inc}}$ described by (20):

$$L_{lt} = L_{l,\text{int}} + L_{l,\text{inc}}. \tag{30}$$

The preceding equations for inductances are evaluated numerically and verified experimentally as follows.

V. Experimental Verification

A 4 × 2 matrix transformer was fabricated from machined MN8CX ferrite (made by Ceramic Magnetics, Inc.) and flex-circuit windings [3]. The values of the core and winding parameters that appear in (4), (7), (18), (23), and (26) are listed in Table I. These values are used to compute the values listed in Table II for the intermediate parameters described by (18), (20), (22), (23), (25), (26), (28), and (29). It is interesting to note that the GMD (0.068 cm) is more than twice the center-to-center distance of the two cross-sections in Fig. 10 ($d + C = 0.031$ cm). The self-inductance of L_1 (12.5 nH) is largest because $a'a$ is longest. Although L_2 (5 nH) is less than half of L_1, its effect is more pronounced in (20) because it carries twice the current of L_1. Among the mutual inductances, M_{12} (5.6 nH) is most significant. In fact, M_{12} completely negates the effect of L_2 in (20), significantly reducing the overall interconnect leakage inductance. The overall interconnect leakage inductance (290 nH), however, is 3.87 times the internal leakage inductance (75 nH)! Thus, interconnect networks with low (leakage) inductance need to be identified for matrix transformers.

Since an unintentional air gap is expected between the uneven mating ferrite surfaces, the minimum value $g_{\min}$ of the air gap g in (7) can not be zero. To determine $g_{\min}$, the magnetizing inductance L_{mt} was measured without any intentional air gaps. As the other inductances, L_{mt} was measured at 1 MHz, using the HP 4194A Impedance/Gain-Phase Analyzer. The measured L_{mt}, 64 μH, was then used in (7) to solve for $g_{\min}$, which turned out to be 10 μm, a typical value. To verify (7), two 1-mil sheets of gapping material were inserted between the top and bottom plates to realize the total g of $2(25.4\,\mu\text{m}) + 10\,\mu\text{m} = 60.8\,\mu\text{m}$ listed in Table I. As is evident from Table III, the measured L_{mt} agrees favorably with the computed value.

Before discussing the experimental data for leakage inductance, it is necessary to point out that because of the way the paralleling strips are constructed and shorted together, their separation d (in Table I and Fig. 10) *varies* along the length of the strips. Each strip is a laminate of a 4.2-mil copper sheet and a 2-mil insulating sheet. The insulating sides were placed facing each other, resulting in the minimum spearation $d_{\min} = 4$ mil. To make the short-circuit between a and b (Fig. 9), the insulating materials were etched away in the vicinity of a and b. A solder ball was then placed between a and b and melted by heat applied to the copper on top of the solder ball, resulting in the maximum separation $d_{\max} = 12$ mil. The d presented in Table I is the average of $d_{\min}$ and $d_{\max}$, which is

TABLE I
PARAMETER VALUES FOR THE FABRICATED 4 × 2 MATRIXTRANSFORMER

Parameter (Equation)	Value	Parameter (Equation)	Value
r_0 (4)	0.463 cm	μ_o (7)	$4\pi 10^{-7}$ H/m
r_i (4)	0.343 cm	μ_r (7)	2050
Postr (4)	0.292 cm	t_p (18)	71.1 μm
Plate (4)	0.229 cm	t_s (18) = C (23)	107 μm
WH (4)	0.176 cm	t_i (18)	50.8 μm
Cl (4)	0.051 cm	B (23)	0.206 cm
g (7)	60.8 μm	d (26)	0.020 cm

TABLE II
INTERMEDIATE VALUES OF I NDUCTANCE CALCULATIONS

Parameter (Equation)	Value	Parameter (Equation)	Value
$L_{l,\text{int}}$ (18)	**75 nH**	M_{12} (25)	5.6 nH
GMR (23)	0.0484 cm	M_{13} (29)	2.6 nH
GMD (26)	0.0680 cm	M_{14} (28)	1.7 nH
L_1 (22)	12.5 nH	M_{24} (29)	1.3 nH
L_2 (22)	5 nH	$L_{l,\text{inc}}$ (20)	**290 nH**

TABLE III
COMPARISON OF COMPUTED AND MEASURED INDUCTANCES

Parameter (Equation)	Value	Parameter (Equation)	Value
$L_{mt,\text{computed}}$ (18)	14.4 μH	$L_{lt,\text{computed}}$ (30)	365 nH
$L_{mt,\text{measured}}$	14.5 μH	$L_{lt,\text{measured}}$	379 nH

8 mil or 0.02 cm. The components of the interconnect leakage inductance due to this value of d are tabulated in Table II. The resulting computed leakage inductance is 365 nH, which is within 5% of the measured value of 379 nH.

VI. CONCLUSION

The *geometrical and constructional features* of a 4 × 2 matrix transformer, which are relevant to inductance modeling, have been reviewed. The core consists of rectangular ferrite plates bridged by cylindrical and semicylindrical ferrite posts. The core construction preserves *magnetic periodicity,* which allows the matrix transformer to be decomposed into identical (or almost-identical) magnetic elements. The windings are made from flex circuits, which are suitable for high-frequency and low-profile requirements. Since the secondary turns are distributed on a planar surface, *interconnecting strips* are needed to parallel these turns.

Thanks to the magnetic periodicity of the core structure, the magnetizing inductance is the sum of the elemental magnetizing inductances of the magnetic elements. The elemental magnetizing inductances are computed by the *reluctance method.*

Because of the interconnecting strips, an *interconnect leakage inductance* is present, in addition to the conventional *internal leakage inductance.* The interconnects contribute as much as 80% of the total leakage inductance.

The *internal leakage inductance* is related to the magnetic energy stored in the winding windows. The magnetic energy is computed from the magnetic field intensity, which is approximated by a function that varies inversely with the radius and linearly along the winding thicknesses.

The *interconnect leakage inductance* is related to the magnetic energy generated by the currents in the interconnecting strips. The magnetic energy is computed from the self-inductances and mutual inductances of the interconnecting conductors, as well as from the nonuniform current distribution among the conductors. The self- and mutual inductances are derived from published tables and formulae.

The modeling methods outlined above predict inductances to within 5% of the measured values. The close agreement between prediction and measurement may be credited both to the validity of the modeling approaches and to the high degree of accuracy (within one mil) with which the core and flex-circuit dimensions can be fabricated.

REFERENCES

[1] E. Herbert, "Flat matrix transformers," United States Patent 4,665,357, May 12, 1987.
[2] K. Sum and E. Herbert, "Novel low-profile matrix transformers for high density power conversion," *Powerconversion and Intelligent Motion,* pp. 102–104, Sept. 1988.
[3] E. Alpizar, K. D. T. Ngo, and J. K. Watson, "Development and characterization of a low-profile matrix transformer," in *Proc. High Frequency Power Conversion Conf.,* 1990, pp. 174–183.
[4] L. F. Casey and M. F. Schlecht, "A high frequency, low volume point-of-load power supply for distributed power systems," *IEEE Power Electron. Spec. Conf. Rec.,* 1987, pp. 439–450.
[5] A. Dauhajre and R. D. Middlebrook, "Modeling and estimation of leakage phenomena in magnetic circuits," *IEEE Power Electron. Spec. Conf. Rec.,* 1986, pp. 213–226.
[6] F. W. Grover, *Inductance Calculations.* Dover Publications, Inc. Reprinted by Instrument Society of America, Research Triangle Park, NC, 1973.
[7] J. K. Watson, *Applications of Magnetism,* 2nd Ed. Gainesville, FL: Author, 1985.
[8] W. H. Hayt, Jr., *Engineering Electromagnetics,* 3rd Ed. New York: McGraw-Hill, 1974.

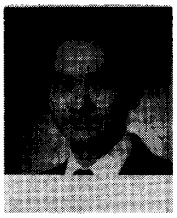

Khai D. T. Ngo (S'82–M'84) received the B.S. degree in electrical and electronics engineering from California State Polytechnic University, Pomona, in 1979, and the M.S. and Ph.D. degrees in the same discipline from California Institute of Technology, Pasadena, in 1980 and 1984, respectively.

He was a Member of Technical Staff at General Electric Corporate Research and Development Center in Schenectady, NY, from 1984 to 1988. He has been an Assistant Professor in the Department of Electrical Engineering at the University of Florida since 1988. His current research interests are in low-profile magnetics, power integrated circuits, power semiconductor devices, and high-frequency converters for utility systems.

E. Alpizar received the B.S. and Licentiate Degrees in electrical engineering from Universidad de Costa Rica in 1974 and 1982, respectively, and the M.S. degree in the same discipline from the University of Florida, Gainesville, in 1990. He worked for industry in Costa Rica from 1975 to 1980. He was an Assistant Professor of Maintenance Engineering at the Instituto Tecnologico de Costa Rica. He is now a faculty member at the Escuela de Ingenieria Electrica of the Univesidad de Costa Rica. His research interest is in power engineering and magnetics.

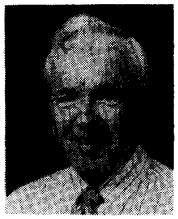

J. Kenneth Watson (M'55–SM'61) received the B.S. degree in electrical engineering from the University of Oklahoma, Norman, in 1951, the S.M. degree from Massachusetts Institute of Technology, Cambridge, MA, in 1955, and the Ph.D. degree from Rice University, Houston, TX, in 1966.

He is on the faculty of the University of Florida where his teaching and research interests are mainly in areas of applied magnetics, now including power electronics. He is the author and publisher of the textbook *Applications of Magnetism* (1985).